

\mathcal{PT} -symmetric trimer systems

L. Jin^{1,*}

¹*School of Physics, Nankai University, Tianjin 300071, China*

We studied parity-time (\mathcal{PT}) symmetric trimer systems that feature open and closed boundaries. The exceptional point is three-state coalescence at zero energy because of chiral symmetry in the open trimer; however, two-state coalescence appears in the closed trimer affected by the magnetic flux enclosed, which suppresses the \mathcal{PT} transition. Dynamics at the phase transition point were also qualitatively studied. For three-state coalescence, the probability of an initial state increases in a power law. The highest order is four; however, it can be reduced to two for the state that is only relevant to one associated state. For two-state coalescence in the trimer ring, we found four typical dynamical behaviors of state probability: (i) unchanged, (ii) oscillation, (iii) quadratic increase, and (iv) quadratic increase with oscillation. The scattering properties of the trimer systems were also studied, particularly, asymmetric wave emissions at spectral singularities.

PACS numbers: 11.30.Er, 42.25.-p, 03.65.Vf, 42.60.Da

I. INTRODUCTION

Parity-time (\mathcal{PT}) symmetric systems possess intriguing features that derive from non-Hermiticity and the \mathcal{PT} symmetry. The \mathcal{PT} -symmetric systems have been extensively investigated, both theoretically [1–20] and experimentally [21–26]. The \mathcal{PT} -symmetry breaking [21–23], nonreciprocal reflectionless [24], and coherent perfect absorber [25–27] have been observed. In 2014, \mathcal{PT} -symmetric systems have been realized by on-chip devices, known as two coupled whispering gallery mode ring microresonators [28–30]. These resonators have high quality factors, and a gain in one resonator, induced by pumping the doped ions, can balance losses in both resonators. The realized \mathcal{PT} -symmetric coupled waveguides and resonators are mainly described by the two-site models, which act as a \mathcal{PT} -symmetric dimer [31]. The two-site dimers are the most concise and simple \mathcal{PT} -symmetric systems, however, all the \mathcal{PT} symmetry breaking [21], power oscillation [22], and gain induced large nonlinearity [23, 28, 30] were found in these systems. Previous study demonstrated the differences of \mathcal{PT} -symmetry and pseudo-Hermiticity in non-Hermitian trimer chain systems [32]. In an optomechanical system coupled with an active resonator, high-order EPs are useful for low-power mechanical cooling [34]. Triple-cavity supermodes was analysed based on the coupled mode theory [33]. Besides, \mathcal{PT} -symmetric oligomers were investigated in nonlinearity systems, the solution and nonlinear dynamics were examined [35, 36]. The asymmetric scattering properties for left and right propagation were demonstrated for nonlinear \mathcal{PT} -symmetric oligomers embedded in linear lead; the plane waves are dynamically unstable except in the vicinity of the linear limit; however, the asymmetric transmissions persist for Gaussian wave packets [37].

This paper focuses on the \mathcal{PT} -symmetric trimer. We

investigated two \mathcal{PT} -symmetric trimer systems under different boundary conditions (one with an open chain form and the other with a closed ring form) and analytically solved their Hamiltonians. We concentrate on dynamics at the \mathcal{PT} -symmetric phase transition (i.e., exceptional) point of trimer systems, particularly in the presence of effective magnetic flux. From the eigen spectrum, we obtained the \mathcal{PT} -symmetric phase transition point and revealed that the uniformly coupled trimer chain with balanced gain and loss at its ends has one exceptional point, where three eigenstates coalesce at zero energy. In the trimer ring, a nonreciprocal coupling connects the head and tail of the trimer chain and the nonreciprocal coupling factors correspond to a gauge invariant field, which can be seen as an effective magnetic flux. For the trimer ring, the \mathcal{PT} -symmetric phase transition point can be a two or three eigenstates coalescence. To determine the dynamical features at the exceptional point in the trimer systems, we examined the time evolution of different initial states. For the trimer chain, the probability increases at the exceptional point in a power law. Because of the three-state coalescence (EP3) [38], the highest order in the power law is four; however, this probability increases quadratically at the EP3 when the initial state is only related to the eigenstate and the first associated state. In the trimer ring, the \mathcal{PT} -symmetric phase transition point is a two-state coalescence (EP2) except for the effective magnetic flux, which is $\Phi = 2n\pi + \pi/2$ ($n \in \mathbb{Z}$). For the EP2, the coalesced two eigenenergy and the third one are all nonzero. The evolved probability of an initial state has four typical behaviors, (i) unchanged, (ii) oscillation, (iii) quadratic increase, and (iv) quadratic increase with oscillation. Notably, the oscillation periods are the same, because they are coalesced eigenenergy dependent, i.e., $2\pi/E_2$. We also investigated the scattering properties of the trimer systems, particularly, the spectral singularities and asymmetric wave emissions under the influence of nonreciprocal coupling.

The remainder of this paper is organized as follows. In Sec. II, we present the trimer systems, the \mathcal{PT} -symmetric phase diagram, and the spectrum. In Sec. III, we inves-

* jinliang@nankai.edu.cn

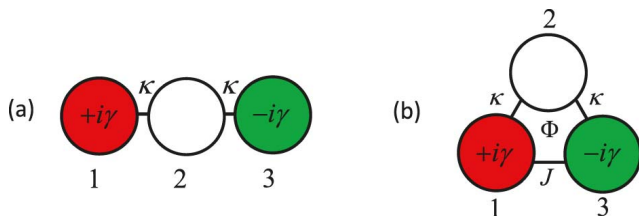


FIG. 1. (Color online) Schematic configuration of trimer systems. (a) A trimer chain with open boundary. (b) A trimer ring with periodical boundary. The trimer systems have a pair of balanced gain (red) and loss (blue).

tigate the dynamics at the exceptional point. In Sec. IV, we explore the scattering properties of the trimer systems, especially the spectral singularities and asymmetric wave emission. Finally in Sec. V, we summarize the results and conclude our study.

II. \mathcal{PT} -SYMMETRIC TRIMER

Open boundary.—The open boundary trimer system has three sites coupled in chain form, with a coupling strength of κ . Specially, the trimer has a gain and loss site coupled to an intermediary site between them. The system is schematically illustrated in Fig. 1(a), and the trimer chain Hamiltonian is

$$H_0 = -\kappa(a_1^\dagger a_2 + a_2^\dagger a_3 + \text{h.c.}) + i\gamma a_1^\dagger a_1 - i\gamma a_3^\dagger a_3, \quad (1)$$

where a_j^\dagger (a_j) is the creation (annihilation) operator of site j and \mathcal{P} is the parity operator, which satisfies $\mathcal{P}a_j^\dagger\mathcal{P}^{-1} = a_{4-j}^\dagger$, $\mathcal{P}a_j\mathcal{P}^{-1} = a_{4-j}$; \mathcal{T} is the time-reversal operator, which satisfies $\mathcal{T}i\mathcal{T}^{-1} = -i$. According to the definitions of the \mathcal{P} and \mathcal{T} operators, the trimer chain Hamiltonian is \mathcal{PT} -symmetric, i.e., $(\mathcal{PT})H_0(\mathcal{PT})^{-1}$. We can also define a unitary transformation S through $Sa_j^\dagger S^{-1} = (-1)^j a_{4-j}^\dagger$ and $Sa_j S^{-1} = (-1)^j a_{4-j}$, where the trimer chain Hamiltonian under the unitary transformation satisfies $SH_0S^{-1} = -H_0$. This indicates that the trimer chain also has a chiral symmetry, and that the spectrum is symmetrical at zero energy. The eigenvalues found are 0 and $\pm\sqrt{2\kappa^2 - \gamma^2}$. All three eigenstates are \mathcal{PT} -symmetric for balanced gain and loss in the region $|\gamma/\kappa| < \sqrt{2}$, and the trimer chain is in the exact \mathcal{PT} -symmetric phase. When $|\gamma/\kappa| > \sqrt{2}$, the \mathcal{PT} symmetry of two eigenstates with imaginary energy $\pm i\sqrt{\gamma^2 - 2\kappa^2}$ breaks, and the trimer chain enters the broken \mathcal{PT} -symmetric phase. By contrast, when $|\gamma/\kappa| = \sqrt{2}$, the trimer chain is at the exceptional point, which is the \mathcal{PT} -symmetric phase transition point [39], where three eigenstates coalesce with zero energy. Notably, this is the only exceptional point in the trimer chain.

Periodical boundary.—A three-site system can also constitute a trimer coupled together in ring form, as schematically illustrated in Fig. 1(b). The Hamiltonian

is denoted as H in the following:

$$H = (-\kappa a_1^\dagger a_2 - \kappa a_2^\dagger a_3 - J e^{i\Phi} a_1^\dagger a_3 + \text{h.c.}) + i\gamma a_1^\dagger a_1 - i\gamma a_3^\dagger a_3, \quad (2)$$

which has an additional nonreciprocal hopping $-J e^{\pm i\Phi}$ between sites 1 and 3 compared with the trimer chain. Moreover, H can be expressed as $H = H_0 - J e^{i\Phi} a_1^\dagger a_3 - J e^{-i\Phi} a_3^\dagger a_1$. The nonreciprocal phase factor $e^{\pm i\Phi}$ is equivalent to an effective magnetic flux Φ enclosed in the trimer ring, which can be introduced in the coupling process through an optical path imbalance method [40]. The trimer ring retains identical \mathcal{PT} symmetry in the presence of the nonreciprocal hopping term; however, the trimer ring is chirally symmetric at magnetic flux $\Phi = n\pi + \pi/2$ ($n \in \mathbb{Z}$), i.e., $SHS^{-1} = -H$. The nonreciprocal coupling enriches the varieties of the trimer spectrum. In particular, the \mathcal{PT} -symmetric transition of the trimer changes considerably.

The trimer ring is a 3×3 matrix. Under the basis $\{a_1^\dagger |\text{vac}\rangle, a_2^\dagger |\text{vac}\rangle, a_3^\dagger |\text{vac}\rangle\}$, H is in the following form:

$$\begin{pmatrix} i\gamma & -\kappa & -J e^{i\Phi} \\ -\kappa & 0 & -\kappa \\ -J e^{-i\Phi} & -\kappa & -i\gamma \end{pmatrix}. \quad (3)$$

The eigenenergy can be analytically determined from the cubic equation $E^3 + (\gamma^2 - J^2 - 2\kappa^2)E + 2J\kappa^2 \cos \Phi = 0$. The \mathcal{PT} symmetry transition point occurs at

$$(\gamma^2 - J^2 - 2\kappa^2)^3 / 3^3 + (2J\kappa^2 \cos \Phi)^2 / 2^2 = 0, \quad (4)$$

which indicates the exceptional points of the trimer ring. Unlike the trimer chain, the exceptional points in the trimer ring can be a coalescence of two eigenstates for effective magnetic flux that is not at half magnetic flux quantum ($\Phi \neq n\pi + \pi/2$, $n \in \mathbb{Z}$).

In Fig. 2, the phase diagram is depicted as a function of coupling strength and gain rate. In the plots, the regions filled with colors represent the exact \mathcal{PT} -symmetric phase for different magnetic fluxes. At trivial magnetic flux $\Phi = 2n\pi$ ($n \in \mathbb{Z}$), the \mathcal{PT} -symmetric phase is portrayed in the yellow areas. At coupling $\kappa = 0$, the trimer ring reduces into a dimer chain with a sole site, and the critical \mathcal{PT} symmetry transition point for the dimer is well known at $\gamma_c = J$. However, at coupling $\kappa = J$, the trimer is a uniform coupled ring, and the \mathcal{PT} symmetry is fragile; any nonzero gain or loss ($\gamma \neq 0$) breaks the \mathcal{PT} symmetry, and eigenenergies of a pair of eigenstates become complex conjugation. *Magnetic flux suppresses the \mathcal{PT} transition.* In the presence of nontrivial magnetic flux $\Phi \neq 2n\pi$ ($n \in \mathbb{Z}$), the \mathcal{PT} -symmetric region enlarges, and the blue areas indicate the additional \mathcal{PT} -symmetric region at $\Phi = 2n\pi + \pi/4$ compared with $\Phi = 2n\pi$ ($n \in \mathbb{Z}$). In this situation, at coupling $\kappa = 0$, the trimer ring reduces into a dimer chain and a sole site, and the critical point is also at $\gamma_c = J$. This reflects how nonreciprocal phase factor $e^{\pm i\Phi}$ has no effect in the dimer chain. By taking a local transformation $a_1^\dagger \rightarrow e^{i\Phi} a_1^\dagger$, $a_1 \rightarrow e^{-i\Phi} a_1$

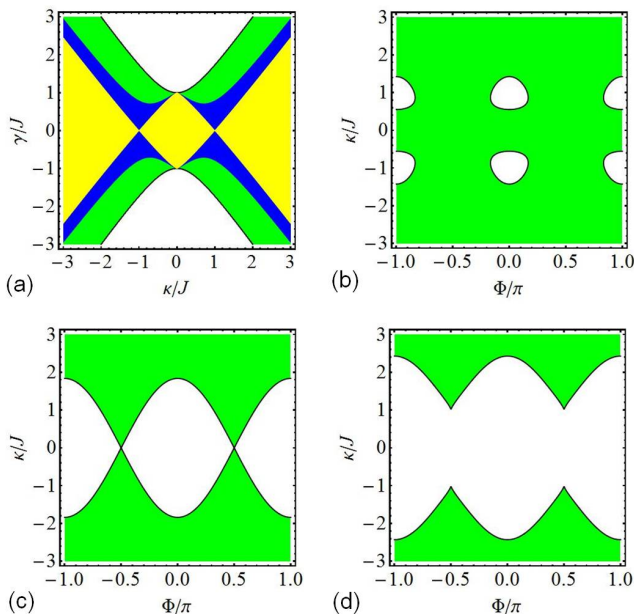


FIG. 2. (Color online) Magnetic flux suppresses the \mathcal{PT} transition. (a) Phase diagram of the trimer ring in the κ and γ plane. The yellow region is the \mathcal{PT} -symmetric phase for $\Phi = 0$. The \mathcal{PT} -symmetric region becomes large as magnetic flux increases, the blue region is the additional \mathcal{PT} -symmetric region for $\Phi = \pi/4$. All the colored regions are for $\Phi = \pi/2$, which shows the \mathcal{PT} -symmetric region at its maximum. (b-d) Phase diagram of the trimer ring in the Φ and κ plane. The green regions are the \mathcal{PT} -symmetric phase for (b) $\gamma/J = 1/2$, (c) $\gamma/J = 1$, and (d) $\gamma/J = \sqrt{3}$.

or $a_3 \rightarrow e^{i\Phi} a_3$, $a_3^\dagger \rightarrow e^{-i\Phi} a_3^\dagger$, the nonreciprocal phase factor $e^{\pm i\Phi}$ in the couplings $J e^{\pm i\Phi}$ is removed. When magnetic flux is $\Phi = 2n\pi + \pi/2$ ($n \in \mathbb{Z}$), the \mathcal{PT} -symmetric region has additional areas highlighted in green compared with $\Phi = 2n\pi + \pi/4$ ($n \in \mathbb{Z}$). The trimer ring has the largest region with exact \mathcal{PT} -symmetric phase. All of the areas in Fig. 2 filled with colors represent the exact \mathcal{PT} -symmetric phase, whereas the white areas are the broken \mathcal{PT} -symmetric phase for half magnetic flux quantum $\Phi = 2n\pi + \pi/2$ ($n \in \mathbb{Z}$).

The critical balanced gain and loss rate is the smallest at coupling $\kappa = 0$ and it increases as the coupling κ in the form of $\gamma_c = \sqrt{J^2 + 2\kappa^2}$. At this \mathcal{PT} -symmetric phase transition point ($\gamma_c = \sqrt{J^2 + 2\kappa^2}$), three eigenstates of the trimer ring coalesce (except for the trimer reduced to a dimer at coupling $\kappa = 0$ ($\gamma_c = J$), which is an EP2). In Figs. 2(b-d), the \mathcal{PT} -symmetric phase diagram in the parameter plane of Φ and κ is plotted. For $|\gamma/J| < 0$, as shown in Figs. 2(b,c), we acquire four typical rules: (i) the \mathcal{PT} -symmetric phase is the most fragile at magnetic flux $\Phi = n\pi$ ($n \in \mathbb{Z}$) and $\kappa/J = 1$; (ii) the exact \mathcal{PT} -symmetric region widens as the magnetic flux increases; (iii) at coupling $\kappa = 0$, magnetic flux does not affect the \mathcal{PT} -symmetric of the trimer ring, and the trimer ring is in the exact \mathcal{PT} -symmetric phase; and (iv) the \mathcal{PT} symmetry is robust at magnetic flux

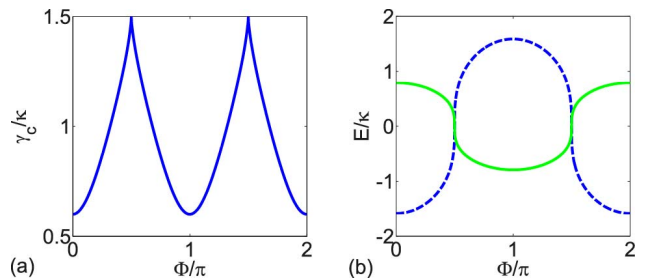


FIG. 3. (Color online) (a) Critical gain and loss of Eq. 5 at EP2, and (b) the spectrum at EP2 as functions of magnetic flux Φ . The green dotted line in (b) represents the two coalesced energies, and the parameters are $\kappa = 1$ and $J = 1/2$.

$\Phi = n\pi + \pi/2$ ($n \in \mathbb{Z}$) and the trimer ring is in the exact \mathcal{PT} -symmetric phase. All four rules remain unchanged as γ increases from 0 to J ; however, the exact \mathcal{PT} -symmetric region shrinks when γ increases. For weak gain and loss $\gamma < J$, the trajectory of exceptional point forms an island with broken \mathcal{PT} symmetry [Fig. 2(b)]. The isolated broken \mathcal{PT} -symmetric region in parameter space was previously found in a dimerized photonic crystals [41], where two kinds of \mathcal{PT} transitions were found: (i) reentering exact \mathcal{PT} -symmetric phase from broken \mathcal{PT} -symmetric phase at higher non-Hermiticity; and (ii) coalescence of EPs from the Brillouin zone center and boundary generates higher order of EPs in the interior of the Brillouin zone [41]. By contrast, we have similar conclusions related to parameters κ and Φ . There are also two kinds of \mathcal{PT} transitions in the trimer ring. (i) As the coupling strength κ increases, the system crosses broken \mathcal{PT} -symmetric phase from exact \mathcal{PT} -symmetric phase and reenters it [Fig. 2(b)]; (ii) EPs from magnetic flux $\Phi = 0$ and $\Phi = \pi$ coalesce and form higher order EPs at $\Phi = \pm\pi/2$ [Figs. 2(c) and 2(d)]. At gain and loss $\gamma = J$, the trimer ring is an EP2 exceptional point at $\kappa = 0$ for any magnetic flux, and the trimer ring is in the exact \mathcal{PT} -symmetric phase at $\Phi = n\pi + \pi/2$ for $\kappa \neq 0$ [Fig. 2(c)]. However, for $|\gamma/J| > 1$, the \mathcal{PT} -symmetric is most robust at $\Phi = n\pi + \pi/2$ ($n \in \mathbb{Z}$). The trimer is \mathcal{PT} -symmetric at $|\kappa/J| > 1$ for $\gamma/J = \sqrt{3}$. As Fig. 2(d) reveals, the trimer ring is in the broken \mathcal{PT} -symmetric region for coupling $|\kappa/J| < 1$ and in the exact \mathcal{PT} -symmetric region for $|\kappa/J| > 2.43$. Additionally, the \mathcal{PT} -symmetric region expands as magnetic flux increases from $\Phi = 2n\pi$ to $\Phi = 2n\pi + \pi/2$ ($n \in \mathbb{Z}$) for the coupling in between $1 < |\kappa/J| < 2.43$, and subsequently shrinks as magnetic flux increases from $\Phi = 2n\pi + \pi/2$ to $\Phi = (2n+1)\pi$ ($n \in \mathbb{Z}$).

In the \mathcal{PT} -symmetric system, the coalesced states encountered are mostly the extensively investigated EP2, which leads to a probability increase under a power law with a highest order of two, $\sum_{n=0}^2 \alpha_n t^n$ [42]. In the open chain form trimer shown in Fig. 1(a), the only exceptional point is an EP3 at $\gamma_c = \sqrt{2}\kappa$. EP3 is a high-order coalescence, where the coalesced states consist of one eigenstate

and two associated states. The probability in the system increases under a power law, and the evolved probability is a polynomial function of time, i.e., $\sum_{n=0}^4 \alpha_n t^n$. Notably, the highest order in the polynomial for EP3 is four. However, in the close ring form trimer shown in Fig. 1(b), two types of coalescence may occur: an EP3 when $\Phi = 2n\pi + \pi/2$ ($n \in \mathbb{Z}$) and $\gamma_c = \sqrt{J^2 + 2\kappa^2}$, or an EP2 when $\Phi \neq 2n\pi + \pi/2$ ($n \in \mathbb{Z}$). Critical gain and loss for the EP2 is

$$\gamma_c = \sqrt{2\kappa^2 + J^2 - 3\sqrt{J\kappa^2 \cos \Phi}^2}, \quad (5)$$

which is plotted in Fig. 3(a) for coupling strengths $\kappa = 1$ and $J = 1/2$ as a function of the effective magnetic flux Φ . The energy spectrum at EP2 is plotted in Fig. 3(b), where two states of three are coalesced; however, at magnetic flux $\Phi = \pi/2$, all three states coalesced. The spectrum is central symmetric at zero energy. When magnetic flux varies from Φ_0 to $\pi - \Phi_0$, the spectrum $E_{1,2}$ is inverted to $-E_{1,2}$. As depicted in Fig. 2(a), the boundaries between regions with different colors indicate when EP2 occurs, whereas the boundaries (black curves) between the colored regions and the white region indicate when EP3 occurs.

The eigenenergies are solved from the cubic equation, and the expressions are complicated. We depict the real and imaginary part of the three band in Fig. 4 for several cases. Specifically, the bands are symmetric with respect to $\Phi = \pi$. In Figs. 4(a) and 4(d), $\gamma = J = \kappa = 1$ [along $\kappa/J = 1$ in Fig. 2(c)], the \mathcal{PT} -symmetric regions in $\Phi \in [0, 2\pi]$ are $1 < \Phi < \pi - 1$ and $\pi + 1 < \Phi < 2\pi - 1$. As effective magnetic flux changes from $\Phi = 0$ to $\Phi = 1$, the two energies with higher real part are the complex conjugate pairs; they change to real energy at $\Phi = 1$ and the system is in the exact \mathcal{PT} -symmetric region during the shift from $\Phi = 1$ to $\Phi = \pi - 1$ with three real energies. The states with the highest and lowest energies continue increasing in this region until $\Phi = \pi - 1$, where the state with the mediate real energy coalesces with the state with the lowest real energy. Subsequently, from $\Phi = \pi - 1$ to $\Phi = \pi$, the higher real energy increases, but the lower two real energies decrease. The conjugate pair is the two states with lower real energy. As Φ changes in the region $[0, \pi]$, the trimer ring transitions from broken \mathcal{PT} -symmetric to exact \mathcal{PT} -symmetric and back to broken \mathcal{PT} -symmetric again. The \mathcal{PT} symmetry transition point is an EP2, and the coalesced energy is nonzero and Φ dependent. In Figs. 4(b) and 4(e), the parameters are given as $\gamma/J = 1 + \cos \Phi$ and $\kappa/J = \cos \Phi$; in this situation, the trimer ring is in the exact \mathcal{PT} -symmetric phase for $\pi/2 < \Phi < 3\pi/2$. By contrast, in Figs. 4(c) and 4(f), the parameters are given as $\gamma/J = 1 - \cos \Phi$ and $\kappa/J = \cos \Phi$, and the trimer ring is in the broken \mathcal{PT} -symmetric phase for $\pi/2 < \Phi < 3\pi/2$.

As all of these figures [Figs. 4(b), 4(c), 4(e), and 4(f)] reveal, the trimer ring experiences three states coalesced \mathcal{PT} symmetry transition points as the parameters change. For $\Phi = \pi$ in Figs. 4(b) and 4(e), the trimer

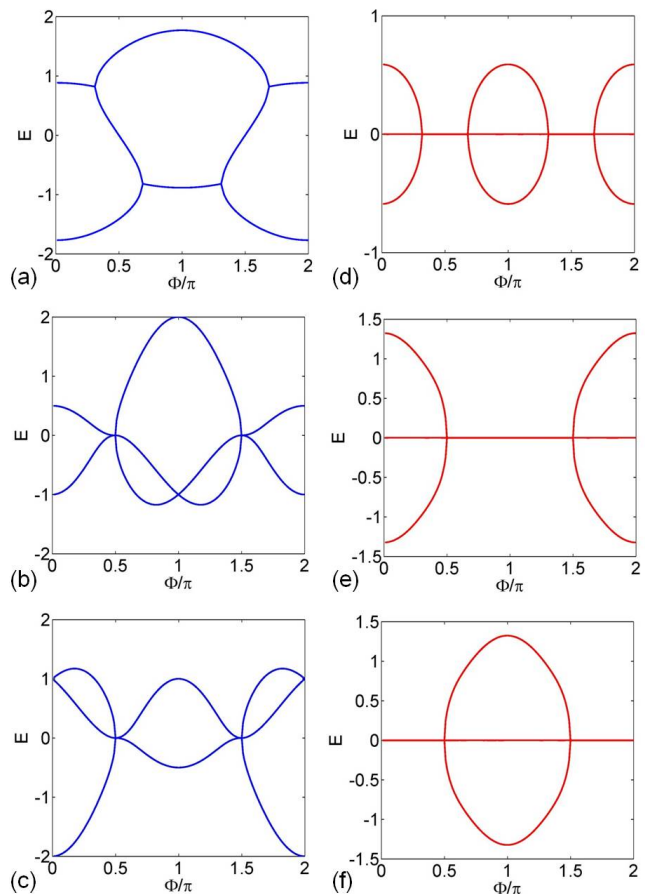


FIG. 4. (Color online) (a-c) Real part (in blue) of the trimer ring spectrum. (d-f) Imaginary part (in red) of the trimer ring spectrum. The parameters are (a,d) $J = \kappa = 1$, (b,e) $\gamma/J = 1 + \cos \Phi$, $\kappa/J = \cos \Phi$, and (c,f) $\gamma/J = 1 - \cos \Phi$, $\kappa/J = \cos \Phi$.

ring is a Hermitian trimer ring with antisymmetric periodical boundary condition at the gain and loss $\gamma = 0$. The energy degeneracy is the traditional degeneracy in Hermitian systems, the same situation which occurs in Figs. 4(c) and 4(f) at $\Phi = 0$.

III. DYNAMICS AT EXCEPTIONAL POINT

The exceptional points universally exist in non-Hermitian systems [43, 44]. Their existence and the role they play for the dynamics of open quantum systems, were investigated by studying the effective Hamiltonian using the Feshbach projection technique. Specifically, the topological structures of the exceptional points significantly affect the dynamical properties [45, 46], and the dynamics at the exceptional points have been investigated in many quantum systems [47–49]. Because of the unique features of the exceptional points, they have been widely applied to sensitivity enhancement [50], parameter estimation [51, 52], and topological energy trans-

fer [53].

Calculation of time evolution.—The Hamiltonian is nondiagonalizable at the exceptional point; instead, changed into a Jordan block form after transformation, namely, $VHV^{-1} = h$, where h is a Jordan block. Generally, h comprises diagonal components (formed by the eigenstates) and Jordan block components (formed by the coalesced states); in other words, h is diagonalized, except for the nondiagonalizable Jordan block components. The differential equations (i.e., the Schrödinger equations) can be solved directly by $id\psi(t)/dt = h\psi(t)$ with $\psi(0) = V^{-1}\Psi(0)$ and the initial state $\Psi(0)$. The diagonalized components correspond to the eigenstates of H , and the time evolution is simply a superposition of the eigenstates with dynamical factor e^{-iEt} , where E is the eigenenergy. For the Jordan block components, the coalesced states are linked in the differential equations, which results in the evolution state in power law of time and the increase of probability. The time evolution can be obtained from $\Psi(t) = V\psi(t)$. Further details about the calculation of time evolution are provided in Appendix.

Open boundary trimer.—We first considered the trimer chain. As discussed in Sec. II, the trimer has a pair of symmetric energy, $\pm\sqrt{2\kappa^2 - \gamma^2}$, and a parameter independent zero energy state protected by chiral symmetry; the trimer is at the exceptional point when $\gamma = \sqrt{2}\kappa$. In this situation, three states coalesce at energy zero and the only eigenstate in \mathcal{PT} -symmetric form is $(1/2)[-i, \sqrt{2}, i]^T$. The time evolution is obtained directly by solving the differential equations from the Schrödinger equations (see Appendix). The coalesced states induce a polynomial power increase of the initial state probability. For instance, the probability of an initial state $\Psi(0) = [1, 0, 0]^T$ is $P(t) = |\Psi(t)|^2 = 1 + 2\sqrt{2}(\kappa t) + 4(\kappa t)^2 + 2\sqrt{2}(\kappa t)^3 + (\kappa t)^4$ as shown in Fig. 5(a). Here, the initial state is related to the eigenstate and its two associated states, which results in the evolved amplitude of the state growing quadratically. Thus, the probability is a function of time in polynomial form $\sum_{n=0}^4 \alpha_n (\kappa t)^n$. During a long time interval, the power law probability increase is the highest order dominant, i.e., $P(t) \approx \alpha_4 (\kappa t)^4$. However, in special situations, an initial state may relevant to the eigenstate and one of its associated states, where the evolved amplitude of the state can linearly increase as time progresses. Therefore, the highest power order of probability increase can be reduced to two. The condition for a quadratical probability increase at EP3 is $\Psi_1(0) + i\sqrt{2}\Psi_2(0) - \Psi_3(0) = 0$. For instance, we consider an initial state $\Psi(0) = [1/\sqrt{2}, 0, 1/\sqrt{2}]^T$, where the evolved probability is $P(t) = 1 + 4(\kappa t)^2$ [Fig. 5(b)].

Periodical boundary trimer.—In the following, we discuss the dynamics of EP3 and EP2 in detail. We considered the EP3 of the closed trimer, which requires the effective flux at a quarter quantum flux $\Phi = 2n\pi + \pi/2$ ($n \in \mathbb{Z}$). In this situation, the trimer is chiral symmetric, and three eigenstates coalesce at

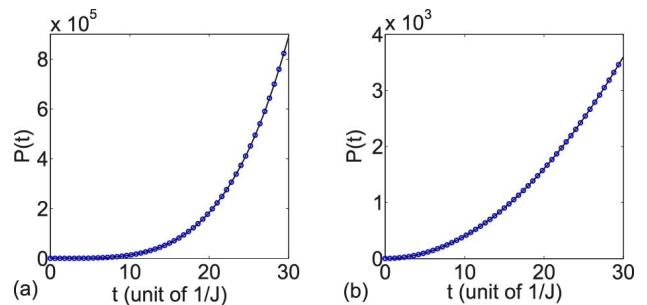


FIG. 5. (Color online) Time evolution probability of the trimer at EP3. (a) Initial state is $|\Psi(0)\rangle = [1, 0, 0]^T$. (b) Initial state is $|\Psi(0)\rangle = [1/\sqrt{2}, 0, 1/\sqrt{2}]^T$. The trimer parameters are $\kappa = 1$ and $\gamma = \sqrt{2}$, and the black lines (blue crosses) are the analytical (numerical) results.

energy zero. The trimer Hamiltonian is nondiagonalizable but can be reduced to a 3×3 Jordan block. The only eigenenergy is zero, and the eigenstate is $\Lambda^{-1/2}[-i\kappa \ J + \sqrt{J^2 + 2\kappa^2} \ i\kappa]^T$, where Λ is the renormalization factor $\Lambda = 2\sqrt{J^2 + 2\kappa^2}(\sqrt{J^2 + 2\kappa^2} + J)$. In Appendix, we describe the procedure by which we obtained the time evolution dynamics. Generally, the initial state probability as a function of time is a polynomial form with no orders larger than four. To interpret the dynamics in detail, we considered a concrete trimer ring with couplings $\kappa = 1$ and $J = 1/2$, and the critical gain and loss of $\gamma_c = 3/2$ under an effective magnetic flux $\Phi = \pi/2$. The only eigenstate for the trimer ring is $(1/\sqrt{6})[-i \ 2 \ i]^T$. Thus, the evolved probability calculated is $P(t) = 1 + 3(\kappa t) + (9/2)(\kappa t)^2 + 3(\kappa t)^3 + (3/2)(\kappa t)^4$ initially for an excitation on the gain site, namely, the state $\Psi(0) = [1, 0, 0]^T$. The probabilities are determined by the evolved state amplitude and can change to other forms for some special initial states. The increases vary in manners; for example, an excitation on the central site (without gain or loss) is $\Psi(0) = [0, 1, 0]^T$ and the probability increase is in an exact quartic form, $P(t) = 1 + \chi(\kappa t)^4$, where the factor χ is coupling strength dependent

$$\chi = \frac{2\kappa^2 + J^2 + J\gamma_c}{\kappa^2 + J^2 + J\gamma_c}. \quad (6)$$

When $\kappa = 1$ and $J = 1/2$, the factor is $\chi = 3/2$, and the probability is $P(t) = 1 + (3/2)(\kappa t)^4$.

Notably, the probability increase at EP3 can be reduced to a quadratic form, just like system at an EP2. For the initial state $\Psi(0) = (1/\sqrt{2})[1, 0, 1]^T$, we calculated the evolved probability, which is $P(t) = 1 + 3(\kappa t)^2$. The condition for a reduced order in the power law probability increase is $\Psi_1(0) + i\sqrt{2}\Psi_2(0) - \Psi_3(0) = 0$ for the trimer ring of $\kappa = 1$, $J = 1/2$, and $\gamma_c = 3/2$ at $\Phi = 2n\pi + \pi/2$ ($n \in \mathbb{Z}$); and the condition changes to $\Psi_1(0) + 2i\Psi_2(0) - \Psi_3(0) = 0$ at $\Phi = 2n\pi - \pi/2$ ($n \in \mathbb{Z}$). In these cases, the highest power of probability increase is two, and it increases monotonically at EP3 for the three

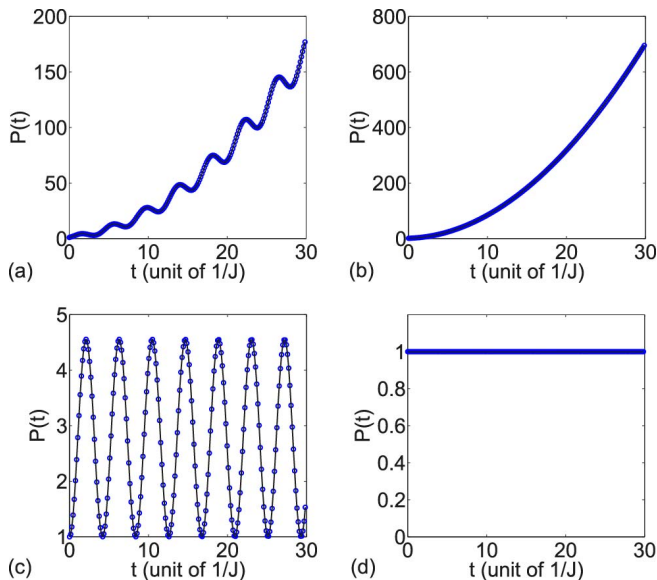


FIG. 6. (Color online) Time evolution probability of the trimer at EP2. Initial state is (a) $|\Psi(0)\rangle = [1, 0, 0]^T$, (b) $|\Psi(0)\rangle = (1/\sqrt{2})[1, -1, 0]^T$, (c) $|\Psi(0)\rangle = (1/\sqrt{3})[1, 1, 1]^T$, and (d) $|\Psi(0)\rangle = (1/\sqrt{2})[1, 0, 1]^T$. The increase in (a, b) is quadratic, and the period in (a, c) is $4\pi/3J$. The trimer parameters are $\kappa = 1/2$, $J = 1$, and $\gamma = \sqrt{3}/2$ at (a-c) $\Phi = -\pi/3$ and at (d) $\Phi = \pi/3$. The black lines (blue crosses) are the analytical (numerical) results.

eigenstates coalescence in the trimer ring. For the trimer ring at EP2 with two eigenstates coalescence, the probability generally increases and oscillates. The oscillation is because of the influence of the third real energy eigenstate. However, special states that are relevant only to the two coalesced states also exist and their probabilities increase monotonically.

The EP2 in the trimer ring occurs when the effective magnetic flux $\Phi \neq 2n\pi + \pi/2$ ($n \in \mathbb{Z}$). The critical value for the balanced gain and loss is revealed in Eq. (5), where we denote E_1 as the energy of the normal eigenstate, and E_2 as the coalesced eigenenergy at EP2, and they satisfy $E_1 = -2E_2$. Considering effective magnetic flux $\Phi = -\pi/3$ as an example, the trimer ring is at the EP2 for the coupling strengths of $J = 1$ and $\kappa = 1/2$, and the critical balanced gain and loss of $\gamma_c = \sqrt{3}/2$. Here, the three eigenenergies are one $E_1 = -1$, and two coalesced energy $E_2 = 1/2$. Generally, the probability of an initial state increases quadratically under an oscillation [Fig. 6(a)]. The oscillation is attributed to the contribution of two different eigenstates (with different real energies E_1 and E_2), the increase results from the two coalesced states (with eigenenergy E_2). Characteristic dynamics emerge in some typical cases, which are determined by the special initial states. When the initial state satisfies $\Psi_1(0) + \Psi_2(0) + \Psi_3(0) = 0$, the contribution of the normal eigenstate E_1 is zero and the probability increases monotonously without oscillation

[Fig. 6(b)]; By contrast, when the initial state satisfies $\Psi_1(0) = \Psi_2(0) = \Psi_3(0)$, this relation leads to the disappearance of the associated states' contribution. Thus, the state probability oscillates in a range rather than increasing with time. The exact expression is $P(t) = [25 - 16 \cos(3t/2)]/9$, as depicted in Fig. 6(c), the period is determined by the energy $T = 2\pi/E_2 = 4\pi/3$. Figure 6(d) shows a probability conservation, which occurs at $\Phi = \pi/3$ for $\Psi(0) = (1/\sqrt{2})[1 \ 0 \ 1]^T$. In this situation, the probabilities at the gain and loss sites remain the same in the time evolution process, and they oscillate at period $T = 4\pi/3$, but the probability for all three sites conserves.

At exceptional points, the system has eigenstates and associated states. All the eigenstates are also \mathcal{PT} -symmetric at exceptional points, while the number of associated states is one less than the coalesced states. In other words, the number of associated states is the same as the number of eigenstates lacking at exceptional points. For the time evolution dynamics, the power oscillation is typically found in the exact \mathcal{PT} -symmetric region; however, when the initial state is only eigenstates relevant at the exceptional point (i.e., not related to the associated state), the probability oscillates instead of increasing.

IV. SCATTERING PROPERTIES

In this section, we studied the scattering properties of the trimers. We considered the trimer embedded in a uniform chain as the scattering center. The coupling strength in the chain is κ , and the left lead is $-\kappa \sum_{j=-\infty}^0 (b_j^\dagger b_{j+1} + b_{j+1}^\dagger b_j)$, whereas the right lead is $-\kappa \sum_{j=1}^{+\infty} (b_j^\dagger b_{j+1} + b_{j+1}^\dagger b_j)$. The operator b_j^\dagger (b_j) is the creation (annihilation) operator in the leads. The input lead is connected to the gain site, whereas the output lead is connected to the lossy site, and the connection Hamiltonian is $-\kappa(b_0^\dagger a_1 + b_1^\dagger a_3 + \text{h.c.})$. Additionally, the scattering wave function in the input lead is denoted as $\langle j | \psi_k \rangle = e^{ikj} + r e^{-ikj}$, whereas in the output lead it is denoted as $\langle j | \psi_k \rangle = t e^{ikj}$, where j is the site number in the input and output lead. $t_{L(R)}$ is the transmission coefficient, and $r_{L(R)}$ is the reflection coefficient for the left (right) side input. The transmission and reflection probabilities are denoted as $T_{L(R)} = |t_{L(R)}|^2$ and $R_{L(R)} = |r_{L(R)}|^2$.

We consider the trimer chain embedded in the lead as a scattering center. The scattering coefficients for input wave vector k are

$$t_L = \frac{i \sin k}{i \sin k - e^{2ik} \gamma^2 \cos k} = t_R, \quad (7)$$

$$r_L = \frac{\gamma^2 \cos k + \gamma \sin(2k)}{i \sin k - e^{2ik} \gamma^2 \cos k}, \quad (8)$$

$$r_R = \frac{\gamma^2 \cos k - \gamma \sin(2k)}{i \sin k - e^{2ik} \gamma^2 \cos k}. \quad (9)$$

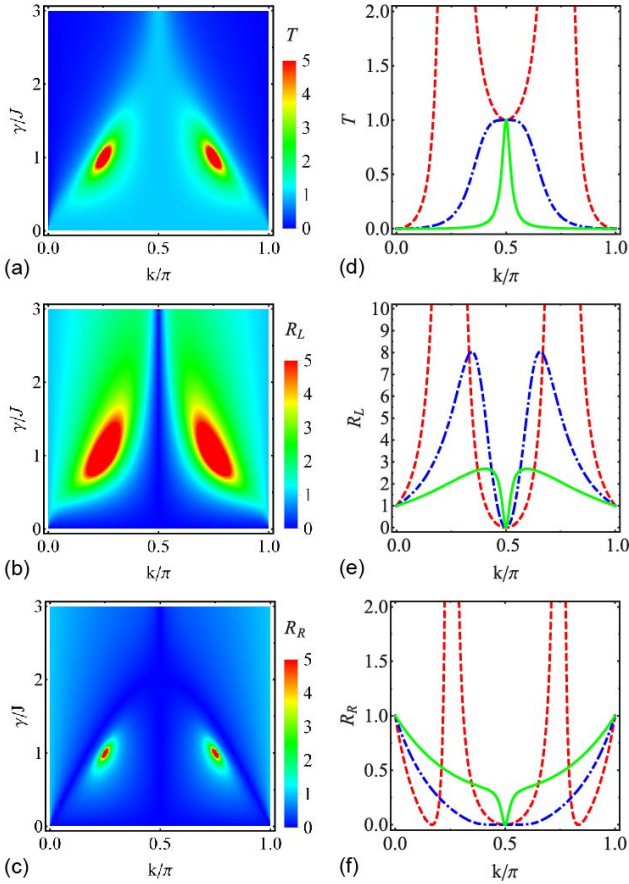


FIG. 7. (Color online) Transmission and reflection probabilities. (a,d) The transmissions, (b,e) the left reflection, and (c,f) the right reflection. (d,e,f) The red dashed, blue dash-dotted, and green solid curves represent $\gamma = \kappa$, $\gamma = 2\kappa$, and $\gamma = 4\kappa$, respectively. The divergence is at $\gamma = \kappa$ for $k = \pi/4$ and $3\pi/4$.

From the expression of the scattering coefficient, the transmission is symmetric (i.e., $T = T_L = T_R$). The transmission coefficients are $t_L = t_R = 1$, and the reflection coefficients are $r_L = r_R = 0$ for input wave vector $k = \pi/2$. Thus, the waves are completely unaffected by the gain and loss. In Fig. 7, the transmission and reflection probabilities are plotted. The transmission is larger than the unity for a wide region of input wave vectors, approximately in the weak gain and loss region $\gamma/J < 1$. For strong gain and loss ($\gamma/J > 2$), the transmission is less than the unity and close to zero in a wide region away from the input wave vector $k = \pi/2$ [Fig. 7(a) and Fig. 7(d)]. Moreover, the left reflection is less than the unity when the wave vector approaches $k = \pi/2$, or at small gain and loss region ($\gamma/J \ll 1$); otherwise, the left transmission is substantially larger than the unity [Fig. 7(b) and Fig. 7(e)]. The right reflection has an opposite law to the left reflection; specifically, the right reflection is usually less than the unity except near the spectral singularities [54–56]. The right reflection also only changes dramatically in close vicinity to the spectral

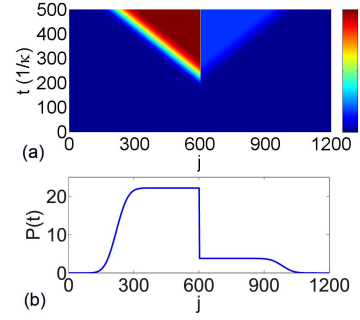


FIG. 8. (Color online) Wave emission dynamics at spectral singularity for the trimer chain. A Gaussian wave packet with $\alpha = 0.02$ centered at $N_c = 900$ is traveling leftward initially, and the trimer chain is at the spectral singularity for $\gamma = \kappa$, $\kappa = \pi/4$. The left-traveling wave height is $\sqrt{\pi}/(4\alpha)$.

singularities [Fig. 7(c) and Fig. 7(f)]. For large $\gamma/J \gg 1$, $R_L R_T \approx 1$ at k deviated from $\pi/2$ and $R_L R_T \approx 0$ at k near $\pi/2$, as indicated by the green lines in Fig. 7(e) and 7(f). In the vicinity of $k = \pi/2$, the transmission is close to the unity and the left and right reflections are near zero.

The scattering system has one spectral singularity at

$$\gamma = \kappa, \quad (10)$$

for input wave vectors $k = \pi/4, 3\pi/4$ (we assume $\kappa, \gamma > 0$) and the waves correspond to energy $E = -\sqrt{2}\kappa$ and velocity $\sqrt{2}\kappa$. At spectral singularity, all of the scattering coefficients diverge, $t_{L,R}, r_{L,R} \rightarrow \infty$. The emission is asymmetric, and the ratio for the right-traveling and left-traveling waves is $3 - 2\sqrt{2} \approx 0.17$. As we numerically simulated the wave emission process depicted in Fig. 8. The initial state is a Gaussian wave packet, $|\Psi(0)\rangle = (\sqrt{\pi}/\alpha)^{-1/2} \sum_j e^{-(\alpha^2/2)(j-N_c)^2} e^{ikj} |j\rangle$ centered at N_c . At the spectral singularities, wave emission toward both sides occurs after the wave packet reaches the trimer scattering center, and it forms a stepped platform. The platform heights for the transmitted part are $\sqrt{\pi}/(4\alpha)$, including the right-traveling wave for the left side input and the left-traveling wave for the right side input. Moreover, after being scattered by the trimer, the left-traveling wave height is $(3 + 2\sqrt{2})\sqrt{\pi}/(4\alpha)$, and the right-traveling wave height is $\sqrt{\pi}/(4\alpha)$ (for left input); by contrast, the left-traveling wave height is $\sqrt{\pi}/(4\alpha)$, and the right-traveling wave height is $(3 - 2\sqrt{2})\sqrt{\pi}/(4\alpha)$ (for the right input). These are revealed by the contour plot in Fig. 8 (a), where the wave emission platform with large height was renormalized to unity. The contour of a left input centered at $N_c = 300$, which is the same as a contour of a right input centered at $N_c = 900$. The initial Gaussian wave packet is centered at $N_c = 900$ in the plot, and it moves from right to left at a velocity $\sqrt{2}\kappa$. Fig. 8(b) details the plotted probability distribution of the wave function at $t = 500/\kappa$, where the asymmetric platform with different heights is clearly observed.

For the trimer embedded in the lead as a scatter-

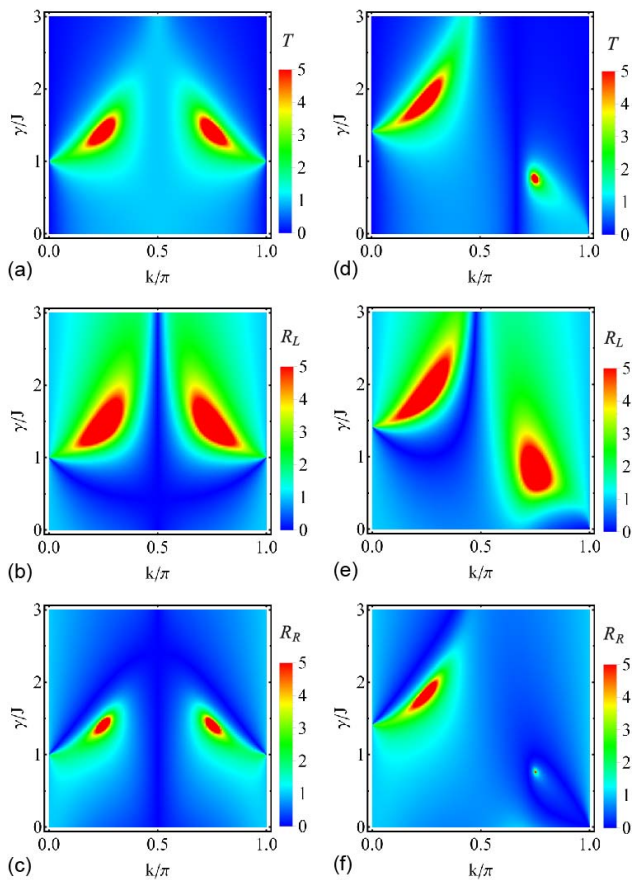


FIG. 9. (Color online) Transmission and reflection probability of the uniform trimer ring ($J = \kappa$) for (a-c) $\Phi = \pi/2$ and (d-f) $\Phi = 0$.

ing center, the scattering coefficients for the input wave vector k are

$$t_L = \frac{i \sin k (e^{-i\Phi} + 2 \cos k)}{ie^{-2ik} \sin k + \cos \Phi + \cos k (1 - \gamma^2)}, \quad (11)$$

$$r_L = \frac{i \sin k (e^{-2ik} - 2i\gamma \cos k)}{ie^{-2ik} \sin k + \cos \Phi + \cos k (1 - \gamma^2)} - 1, \quad (12)$$

$$t_R = \frac{i \sin k (e^{i\Phi} + 2 \cos k)}{ie^{-2ik} \sin k + \cos \Phi + \cos k (1 - \gamma^2)}, \quad (13)$$

$$r_R = \frac{i \sin k (e^{-2ik} + 2i\gamma \cos k)}{ie^{-2ik} \sin k + \cos \Phi + \cos k (1 - \gamma^2)} - 1. \quad (14)$$

where the coupling strengths satisfy $J = \kappa$. From the expressions of the scattering coefficients, the transmission is symmetric (i.e., $T = T_L = T_R$). Figure 9 illustrates the plotted transmission and reflection probabilities. In the region $k \in [0, \pi]$, the scattering probability is symmetrical at $k = \pi/2$ for effective magnetic $\Phi = 2n\pi + \pi/2$ ($n \in \mathbb{Z}$) [Fig. 9(a-c)], where the trimer ring possesses chiral symmetry and its spectrum is symmetrical at zero energy (i.e., the energy $-2 \cos(\pi/2)$). In other magnetic fluxes, such as $\Phi = 0$, the chiral symmetry of the trimer ring

breaks, and the scattering probabilities are asymmetric at $k = \pi/2$ [Fig. 9(d-f)]. When $k = \pi/2$, the reflection and transmission are identical, both symmetrical and γ -independent, $T_L = R_L = T_R = R_R = (\cos^2 \Phi + 1)^{-1}$. The divergence of the scattering coefficients occurs only for wave vectors $k = \pi/4$ and $3\pi/4$. At $k = \pi/4$, the transmissions (t_L and t_R) are larger than zero under any balanced trimer gain and loss γ or when the effective magnetic flux Φ enclosed. The scattering coefficients divergence emerges at

$$\gamma^2 = \sqrt{2} \cos \Phi + 2, \quad (15)$$

and the spectral singularity emerges in the region $\sqrt{2} - \sqrt{2} \leq |\gamma/\kappa| \leq \sqrt{2} + \sqrt{2}$. Notably, the trimer acts as a wave emitter at the spectral singularities. The wave emission is asymmetric, and the contrast ratio of left-traveling wave emission over right-traveling wave emission is $(\sqrt{2}\gamma - 1)/(\sqrt{2}\gamma + 1)$, which is obtained by comparing the transmission and reflection probabilities. The contrast ratio less than one is related to left side with the gain resonator having a larger emission rate. For example, at $\gamma = \sqrt{2}$, $\Phi = \pi/2$, we have $T_L/R_L = 1/3$, $T_R/R_R = 3$. This indicates that the lasing to different directions have different intensities, similar to the trimer chain. The lasing generates three times as many left-traveling waves than does the right-traveling wave. For either the trimer chain or the trimer ring, the asymmetric lasing intensity are both stronger right-traveling waves.

V. CONCLUSION

Two \mathcal{PT} -symmetric trimer systems, comprising an open trimer chain and a closed trimer ring were examined in this study. First, we investigated the spectra of the trimer systems and obtained the \mathcal{PT} -symmetric phase diagram. we found that the nontrivial magnetic flux suppresses the \mathcal{PT} transition. For the trimer chain, the \mathcal{PT} -symmetric phase transition point is an EP3 with three states coalescence; for the trimer ring, except for the EP3, the \mathcal{PT} -symmetric phase transition point can be an EP2 with two states coalescence as long as an effective magnetic flux breaks the chiral symmetry of the trimer ring. Second, we studied the time evolution at the exceptional point in detail, and determined that the state probability can change in four ways when the trimer ring is at EP2: (i) unchanged, (ii) oscillation, (iii) power law increase, and (iv) power law increase with oscillation. These occur because of the nonzero coalesced eigenstate and the third normal eigenstate. Finally, we investigated the scattering properties of the trimer systems with the gain and loss sites embedded in the lead, and calculated the transmissions and reflections for the left- and right-side inputs. Notably, the transmission is symmetric and the reflection is asymmetric. We also found the spectral singularities, at which wave emission is asymmetric. The critical dynamics at exceptional points and the scatter-

ing properties at spectral singularities may be useful in quantum metrology in the future.

Note added: We become aware of a related work, the dynamics in the exact and broken \mathcal{PT} -symmetric phases were investigated in an open trimer chain [57].

ACKNOWLEDGMENTS

We acknowledge the support of National Natural Science Foundation of China (Grant No. 11605094) and the Tianjin Natural Science Foundation (Grant No. 16JCY-BJC40800).

Appendix A: Dynamics at exceptional points

For the trimer ring at EP3, the Hamiltonian at critical gain and loss $\gamma_c = \sqrt{J^2 + 2\kappa^2}$ is in the form of

$$H = \begin{pmatrix} i\sqrt{J^2 + 2\kappa^2} - \kappa & iJ & \\ -\kappa & 0 & -\kappa \\ -iJ & -\kappa & -i\sqrt{J^2 + 2\kappa^2} \end{pmatrix}. \quad (\text{A1})$$

The Hamiltonian can be transformed to $H = VhV^{-1}$ with the transformation

$$V = \begin{pmatrix} -\kappa^2 & i\sqrt{J^2 + 2\kappa^2} & 1 \\ -i\kappa(J + \sqrt{J^2 + 2\kappa^2}) & -\kappa & 0 \\ \kappa^2 & iJ & 0 \end{pmatrix}, \quad (\text{A2})$$

and h is a 3×3 Jordan block with diagonal elements $\lambda = 0$,

$$h = \begin{pmatrix} \lambda & 1 & 0 \\ 0 & \lambda & 1 \\ 0 & 0 & \lambda \end{pmatrix}. \quad (\text{A3})$$

The Schrödinger equations are

$$\frac{id}{dt} \begin{pmatrix} \Psi_1 \\ \Psi_2 \\ \Psi_3 \end{pmatrix} = H \begin{pmatrix} \Psi_1 \\ \Psi_2 \\ \Psi_3 \end{pmatrix}, \quad (\text{A4})$$

substituting $H = VhV^{-1}$, we obtain

$$\frac{id}{dt} V^{-1} \begin{pmatrix} \Psi_1 \\ \Psi_2 \\ \Psi_3 \end{pmatrix} = hV^{-1} \begin{pmatrix} \Psi_1 \\ \Psi_2 \\ \Psi_3 \end{pmatrix}, \quad (\text{A5})$$

by setting $\psi = V^{-1}\Psi$, the Schrödinger equations are reduced to differential equations of ψ , in the form of

$$\frac{id}{dt} \begin{pmatrix} \psi_1 \\ \psi_2 \\ \psi_3 \end{pmatrix} = h \begin{pmatrix} \psi_1 \\ \psi_2 \\ \psi_3 \end{pmatrix}, \quad (\text{A6})$$

which are

$$\frac{id\psi_1}{dt} = \lambda\psi_1 + \psi_2, \quad (\text{A7})$$

$$\frac{id\psi_2}{dt} = \lambda\psi_2 + \psi_3, \quad (\text{A8})$$

$$\frac{id\psi_3}{dt} = \lambda\psi_3. \quad (\text{A9})$$

From the last equation, we get

$$\psi_3 = c_3 e^{-i\lambda t}, \quad (\text{A10})$$

thus, we have $id\psi_2/dt = \lambda\psi_2 + c_3 e^{-i\lambda t}$, and then we get

$$\psi_2 = c_2 e^{-i\lambda t} + (-it) c_3 e^{-i\lambda t}, \quad (\text{A11})$$

consequently, we have $id\psi_1/dt = \lambda\psi_1 + c_2 e^{-i\lambda t} + (-it) c_3 e^{-i\lambda t}$ and

$$\psi_1 = c_1 e^{-i\lambda t} + (-it) c_2 e^{-i\lambda t} - (t^2/2) c_3 e^{-i\lambda t}. \quad (\text{A12})$$

The obtained wave function $\psi(t)$ is

$$\psi(t) = e^{-i\lambda t} \begin{pmatrix} c_1 + (-it) c_2 - (t^2/2) c_3 \\ c_2 + (-it) c_3 \\ c_3 \end{pmatrix}. \quad (\text{A13})$$

Thus, the time evolution state is $\Psi(t) = V\psi(t)$. The coefficients $c_{1,2,3}$ are determined from the initial state. At $t = 0$, we have $\Psi(0) = V\psi(0)$, therefore, the initial state is expressed as

$$\Psi(0) = \begin{pmatrix} \Psi_1 \\ \Psi_2 \\ \Psi_3 \end{pmatrix} = V \begin{pmatrix} c_1 \\ c_2 \\ c_3 \end{pmatrix}, \quad (\text{A14})$$

the coefficients satisfy $(c_1 \ c_2 \ c_3)^T = V^{-1}(\Psi_1 \ \Psi_2 \ \Psi_3)^T$, and the time evolution state $\Psi(t)$ is determined, as

$$\Psi(t) = e^{-i\lambda t} V \begin{pmatrix} c_1 + (-it) c_2 - (t^2/2) c_3 \\ c_2 + (-it) c_3 \\ c_3 \end{pmatrix}. \quad (\text{A15})$$

Here, $\lambda = 0$ for the three states coalescence in the trimer ring.

For the trimer ring at EP2 at magnetic flux $\Phi = \pi/3$, the coupling strengths are $\kappa = 1$ and $J = 1/2$, at critical gain and loss $\gamma_c = \sqrt{3}/2$, the Hamiltonian is in the form of

$$H = \begin{pmatrix} i\sqrt{3}/2 & -1/2 & -e^{i\pi/3} \\ -1/2 & 0 & -1/2 \\ -e^{-i\pi/3} & -1/2 & -i\sqrt{3}/2 \end{pmatrix}, \quad (\text{A16})$$

The Hamiltonian can be transformed to $H = VhV^{-1}$ with

$$V = \begin{pmatrix} 1 - \frac{2}{3}i\sqrt{3} & \frac{1}{2}i\sqrt{3} & 2 + \frac{2}{3}i\sqrt{3} \\ 1 - \frac{2}{3}i\sqrt{3} & -i\sqrt{3} & -1 + \frac{2}{3}i\sqrt{3} \\ 1 - \frac{2}{3}i\sqrt{3} & \frac{1}{2}i\sqrt{3} & -1 + \frac{2}{3}i\sqrt{3} \end{pmatrix}, \quad (\text{A17})$$

and

$$h = \begin{pmatrix} -1 & 0 & 0 \\ 0 & \frac{1}{2} & 1 \\ 0 & 0 & \frac{1}{2} \end{pmatrix}. \quad (\text{A18})$$

At $\Phi = -\pi/3$, $\kappa = 1$, $J = 1/2$, and $\gamma_c = \sqrt{3}/2$, the trimer ring is still an EP2, a transformation is

$$V = \begin{pmatrix} 1 - \frac{2}{3}i\sqrt{3} & \frac{1}{2}i\sqrt{3} & 2 + \frac{2}{3}i\sqrt{3} \\ 1 & 0 & -1 \\ 1 + \frac{2}{3}i\sqrt{3} & -\frac{1}{2}i\sqrt{3} & -1 - \frac{2}{3}i\sqrt{3} \end{pmatrix}, \quad (\text{A19})$$

and h is identical with Eq. (A18). The time evolution

is calculated by the same method introduced in this Appendix.

-
- [1] C. M. Bender and S. Boettcher, Phys. Rev. Lett. **80**, 5243 (1998).
- [2] P. Dorey, C. Dunning, and R. Tateo, J. Phys. A **34**, 5679 (2001).
- [3] C. M. Bender, D. C. Brody, and H. F. Jones, Phys. Rev. Lett. **89**, 270401 (2002).
- [4] A. Mostafazadeh, J. Math. Phys. **43**, 205 (2002).
- [5] H. F. Jones, J. Phys. A **38**, 1741 (2005).
- [6] R. El-Ganainy, K. G. Makris, D. N. Christodoulides, and Z. H. Musslimani, Opt. Lett. **32**, 2632 (2007).
- [7] K. G. Makris, R. El-Ganainy, D. N. Christodoulides, and Z. H. Musslimani, Phys. Rev. Lett. **100**, 103904 (2008).
- [8] Z. H. Musslimani, K. G. Makris, R. El-Ganainy, and D. N. Christodoulides, Phys. Rev. Lett. **100**, 030402 (2008).
- [9] M. Znojil, Phys. Rev. D **78**, 025026 (2008).
- [10] S. Klaiman, U. Günther, and N. Moiseyev Phys. Rev. Lett. **101**, 080402 (2008).
- [11] O. Bendix, R. Fleischmann, T. Kottos, and B. Shapiro, Phys. Rev. Lett. **103**, 030402 (2009).
- [12] L. Jin and Z. Song, Phys. Rev. A **80**, 052107 (2009).
- [13] S. Longhi, Phys. Rev. A **81**, 022102 (2010).
- [14] Y. N. Joglekar, D. Scott, M. Babbey, and A. Saxena, Phys. Rev. A **82**, 030103(R) (2010).
- [15] J. Gong and Q. H. Wang, Phys. Rev. A **82**, 012103 (2010).
- [16] D. C. Brody and E.-M. Graefe, Phys. Rev. Lett. **109**, 230405 (2012).
- [17] P. Ambichl, K. G. Makris, L. Ge, Y. Chong, A. D. Stone, and S. Rotter, Phys. Rev. X **3**, 041030 (2013).
- [18] S. Malzard, C. Poli, and H. Schomerus, Phys. Rev. Lett. **115**, 200402 (2015)
- [19] K. Ding, G. Ma, M. Xiao, Z. Q. Zhang, and C. T. Chan, Phys. Rev. X **6**, 021007 (2016)
- [20] S. Phang, A. Vukovic, S.C. Creagh, P.D. Sewell, G. Gradoni, T.M. Benson, Sci. Rep **6**, 20499 (2016).
- [21] A. Guo, G. J. Salamo, D. Duchesne, R. Morandotti, M. Volatier-Ravat, V. Aimez, G. A. Siviloglou, and D. N. Christodoulides, Phys. Rev. Lett. **103**, 093902 (2009).
- [22] C. E. Rüter, K. G. Makris, R. El-Ganainy, D. N. Christodoulides, M. Segev, and D. Kip, Nat. Phys. **6**, 192 (2010).
- [23] B. Peng, S. K. Özdemir, F. Lei, F. Monifi, M. Gianfreda, G. L. Long, S. Fan, F. Nori, C. M. Bender and L. Yang, Nat. Phys. **10**, 394 (2014).
- [24] L. Feng, Y. L. Xu, W. S. Fegadolli, M. H. Lu, J. E. B. Oliveira, V. R. Almeida, Y. F. Chen, and A. Scherer, Nat. Mater. **12**, 108 (2013).
- [25] Y. Sun, W. Tan, H.-Q. Li, J. Li, and H. Chen, Phys. Rev. Lett. **112**, 143903 (2014).
- [26] W. Wan, Y. Chong, L. Ge, H. Noh, A. D. Stone, H. Cao, Science **331**, 889 (2011).
- [27] Y. D. Chong, L. Ge, H. Cao, and A. D. Stone. Phys. Rev. Lett. **105**, 053901 (2010).
- [28] L. Chang, X. Jiang, S. Hua, C. Yang, J. Wen, L. Jiang, G. Li, G. Wang, and M. Xiao, Nat. Photon. **8**, 524 (2014).
- [29] B. Peng, S. K. Özdemir, S. Rotter, H. Yilmaz, M. Liertzer, F. Monifi, C. M. Bender, F. Nori, and L. Yang, Science **346**, 328 (2014).
- [30] H. Jing, S. K. Özdemir, X.-Y. Lü, J. Zhang, L. Yang, and F. Nori, Phys. Rev. Lett. **113**, 053604 (2014).
- [31] I. Rotter and J. P. Bird, Rep. Prog. Phys. **78**, 114001 (2015).
- [32] S. V. Suchkov, F. Fotsa-Ngaffo, A. Kenfack-Jiotsa, A. D. Tikeng, T. C. Kofane, Y. S. Kivshar, and A. A. Sukhorukov, New J. Phys. **18**, 065005 (2016).
- [33] C. Yang, Y. Hu, X. Jiang and M. Xiao, Phys. Rev. A **95**, 033847 (2017).
- [34] H. Jing, S. K. Özdemir, H. Lü and F. Nori, arXiv:1609.01845 (2016).
- [35] K. Li and P. G. Kevrekidis, Phys. Rev. E **83**, 066608 (2011).
- [36] M. Duanmu, K. Li, R. L. Horne, P. G. Kevrekidis, and N. Whitaker, Phil. Trans. R. Soc. A **371**, 20120171 (2013).
- [37] J. D'Ambroise, P. G. Kevrekidis, and S. Lepri, J. Phys. A: Math. Theor. **45**, 444012 (2012).
- [38] G. Demange and E.-M. Graefe, J. Phys. A: Math. Theor. **45**, 025303 (2012).
- [39] W. D. Heiss J. Phys. A: Math. Theor. **45**, 444016 (2012).
- [40] M. Hafezi, Phys. Rev. Lett. **112**, 210405 (2014).
- [41] K. Ding, Z. Q. Zhang, and C. T. Chan, Phys. Rev. B **92**, 235310 (2015).
- [42] H. Cartarius and N Moiseyev, Phys. Rev. A **84**, 013419 (2011).
- [43] W. D. Heiss, Czech. J. Phys. **54**, 1091 (2004).
- [44] W. D. Heiss, J. Phys. A: Math. Gen. **37**, 2455 (2004).
- [45] M. Müller and I. Rotter, J. Phys. A: Math. Theor. **41**, 244018 (2008).
- [46] I. Rotter, J. Phys. A: Math. Theor. **42**, 153001 (2009).
- [47] R. Uzdin, E. G. Dalla Torre, R. Kosloff, and N. Moiseyev, Phys. Rev. A **88**, 022505 (2013).
- [48] S. Longhi, Eur. Phys. Lett. **106**, 34001 (2014).
- [49] I. Haritan, I. Gilary, Z. Amitay, and N. Moiseyev, J. Chem. Phys. **143**, 154308 (2015).
- [50] J. Wiersig Phys. Rev. Lett. **112**, 203901 (2014).
- [51] M. Am-Shallem, R. Kosloff, and N. Moiseyev, New J. Phys. **17**, 113036 (2015).
- [52] M. Am-Shallem, R. Kosloff, and N. Moiseyev, Phys. Rev. A **93**, 032116 (2016).
- [53] H. Xu, D. Mason, L. Jiang, and J. G. E. Harris, Nature **537**, 80 (2016).
- [54] A. Mostafazadeh, Phys. Rev. Lett. **102**, 220402 (2009).
- [55] A. Mostafazadeh, Phys. Rev. A **87**, 063838 (2013).
- [56] G. R. Li, X. Z. Zhang, and Z. Song, Ann. Phys. **349**, 288 (2014).
- [57] L. F. Xue, T. Tian, H. B. Zhu, and Z. H. Wang, arXiv:1612.06959 (2016).